

## Research Article

### An Analysis of Velocity-temperature Characteristics of Liquid-solid Two-phase Abrasive Flow Machining of Food Molding Tubes

Junye Li, Fengyu Sun, Jing Li, Xuechen Zhang, Ying Xu and Jinlong Wang

College of Mechanical and Electric Engineering, Changchun University of Science and Technology, Changchun 130022, Jilin, China

**Abstract:** In this study, through numerical simulation of solid-liquid two-phase flow heat transfer characteristics of abrasive flow of food molding polishing and corresponding surface machining features of channel inside of common-rail tube, the distributed cloud maps of the dynamic pressure, turbulence kinetic energy, velocity and the static temperature at the regions close to the wall when the temperature and velocity changes can be obtained. Which provide theoretical basis for the realization of surface quality control technology to the food molding tube abrasive flow of food molding polishing. The food molding tube is widely used in military and civil field, the surface quality of the internal channels will decide the performance of the components or the whole machine, abrasive flow of food molding machining technology is an effective method to improve the internal surface quality of food molding tubes.

**Keywords:** Food molding machining, food molding tube, liquid-solid two-phase flow

## INTRODUCTION

The food molding tube used in this research is the common-rail part which is an important part of engine fuel supply system. It has high hardness, low surface roughness, with fillet in the oil outlet cross section, pipe internal surface is smooth and without burrs (Zheng *et al.*, 2012; Li *et al.*, 2014). According to the data provided by the enterprise, the selected common-rail pipe parts geometric model entrance one 16 diameter, branch diameter is 4mm (Liu *et al.*, 2012). The three-dimensional model of the common-rail pipe parts of is shown in Fig. 1 (Walia *et al.*, 2008).

According to the velocity distribution maps, the velocity was relatively large at the hole intersection. As a result of the extruding and grinding action of abrasive flow of food molding, larger fillets will be made in this region, which will effectively reduce the fatigue stress caused by the high pulse and significantly improve the fatigue strength of common rail. This machining method can produce a finished surface, enhance the reliability of parts and prolong the service life.

## MATERIALS AND METHODS

**Numerical analysis:** Because of abrasive flow of food molding is viscous fluid, to study the heating, heat transfer in the process of common-rail pipe abrasive flow of food molding polishing, we need to analysis the parameters, such as the dynamic pressure and the



Fig. 1: The common-rail pipe parts model

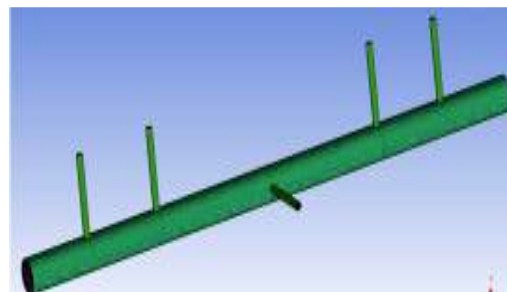


Fig. 2: The situation of the part meshing

turbulence kinetic energy of near wall area of the be machined part. The internal channel structure of common-rail pipe is relatively simple, using the unstructured hexahedron meshing (Sankar *et al.*, 2010, 2011), the situation of the divided grid is shown in Fig. 2.

The quality of meshing will directly affect the required computing resources configuration and the convergence of the simulation results, the calculation accuracy, check the common indicators of unstructured

**Corresponding Author:** Junye Li, College of Mechanical and Electric Engineering, Changchun University of Science and Technology, Changchun 130022, Jilin, China

This work is licensed under a Creative Commons Attribution 4.0 International License (URL: <http://creativecommons.org/licenses/by/4.0/>).

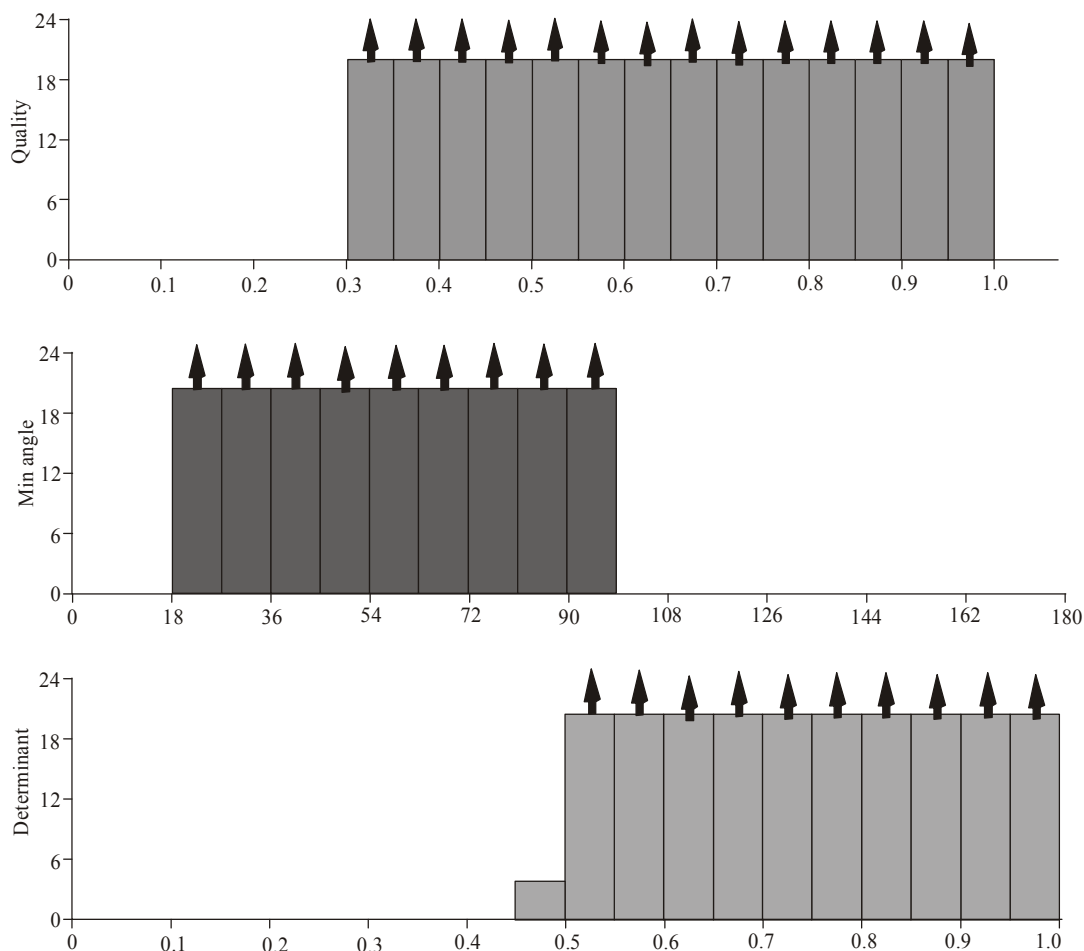


Fig. 3: The mesh quality check

mesh quality in order to obtain a satisfactory quality of grid (Jain and Jain, 2000, 2001, 2004), the mesh of U-tube geometry model and mesh quality inspection situation is shown in Fig. 3.

### RESULTS AND DISCUSSION

The numerical simulation of the common rail 3D channel model was made in two modes (different initial temperatures and the same inlet velocity vs. different inlet velocities and the same initial temperature) and after the calculation, their residual error curves are shown in Fig. 4.

Figure 4 shows that convergence occurs after about 88 iterations, indicating that the common-rail channel model is designed and the calculation parameters are set reasonably, through which the convergence can be reached. In view of the characteristics of this physical model, the flow characteristics of the abrasive flow of food molding in common-rail channel were obtained mainly from the comparative analysis of the factors affecting the turbulence pattern of abrasive flow of food molding. In order to make the best analysis of the

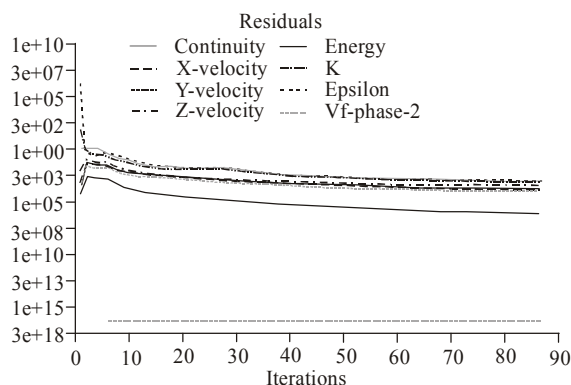


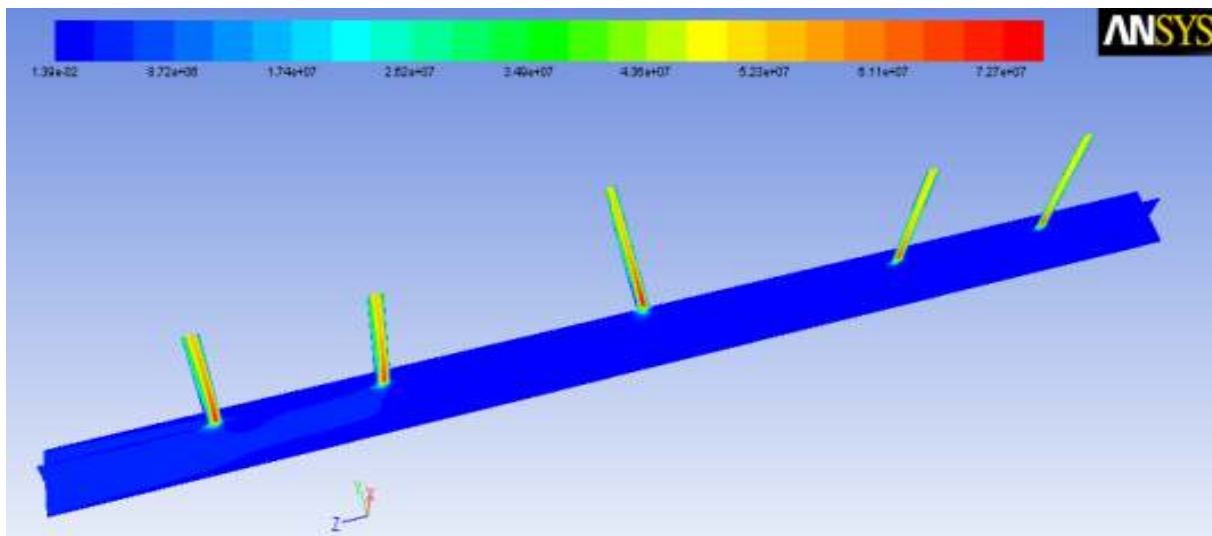
Fig. 4: The calculation residual error curve of common-rail channel

characteristics of the abrasive flow of food molding machining flow field, the simulation results on surface XOZ and surface YOZ were displayed. With an inlet velocity of 60 m/s and the initial temperatures set at 290, 300, 310, 320, 330 and 340 K, respectively, the synchronous machining of five branches was simulated, thus producing the distributed cloud maps of dynamic pressure and velocity as shown in Fig. 5.

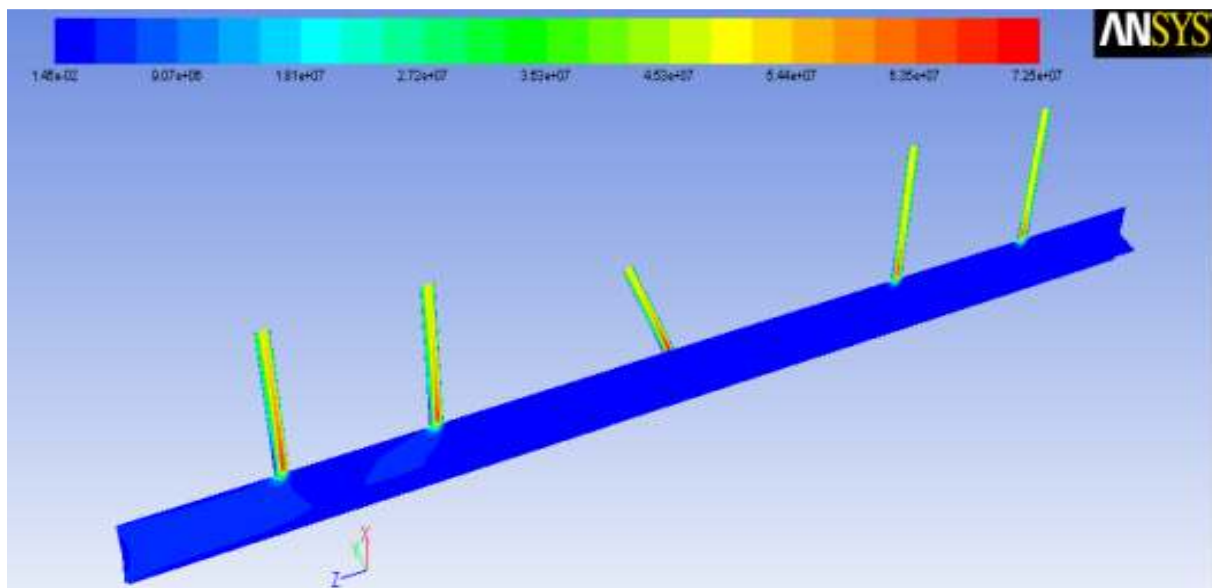
Figure 5 shows that, in the trunk of the common-rail channel, the dynamic pressure from the inlet to a certain region was relatively large, but it declined with the advance of the flow. This can be attributed to the energy loss of the abrasive flow of food molding due to viscosity and particle collisions or other factors during the flowing course. The dynamic pressure in the branches of the common-rail channel was greater than that in the trunk: the closer the regions were to the branch center, the greater the dynamic pressure was and it grew to the maximum at the cross hole. This is caused by the sudden decrease in the cross section of common-rail branches and the direction change of abrasive flow of food molding in the channel. Figure 6 shows that dynamic pressure distribution differed in the five branches: the closer the branch was to the inlet, the

better its internal dynamic pressure distribution was. However, the dynamic pressure in common-rail channel did not change much as the temperature increased; as the temperature increased, the gap between dynamic pressures narrowed slightly.

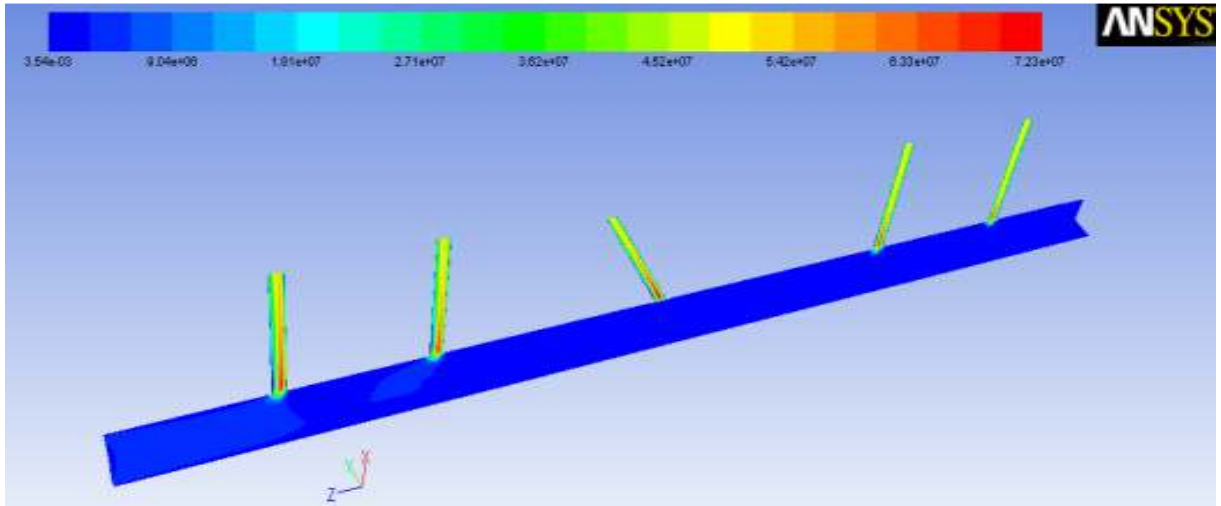
When observing the turbulence kinetic energy maps, we can find that turbulence kinetic energy was distributed regionally in 4 zones: zone 1, 2, 3 and 4 from the bottom to the top. In order to facilitate the comparative observation, the dynamic pressure maps were divided into 4 zones in the same way: zone 1, 2, 3 and 4. Next, an in-depth comparison was made between the turbulence kinetic energy and dynamic pressure at the regions close to the wall of common-rail branches. The distribution of the turbulence kinetic energy and



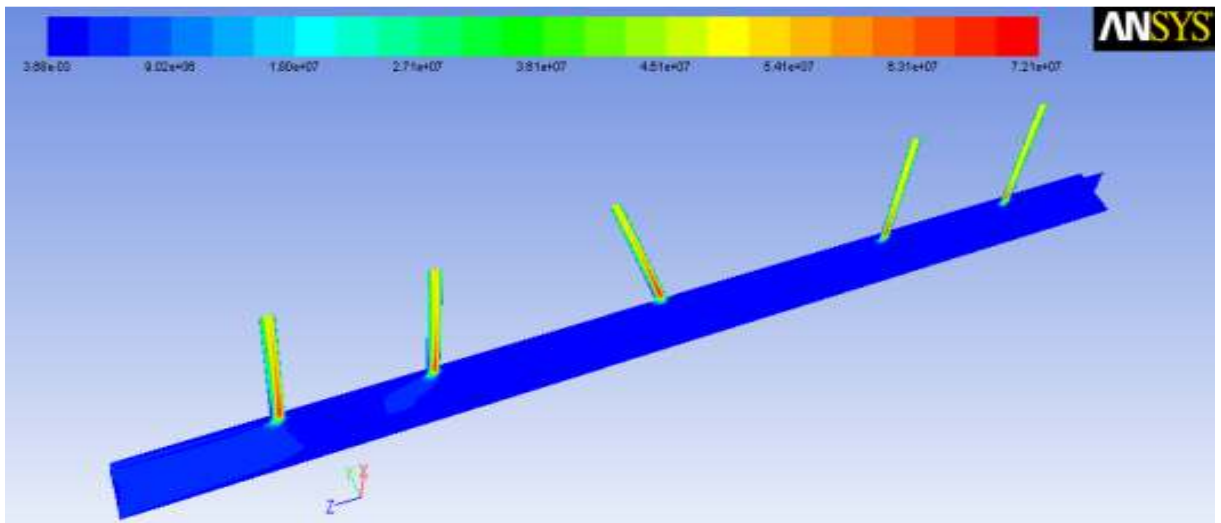
(a) Temperature of 290 K



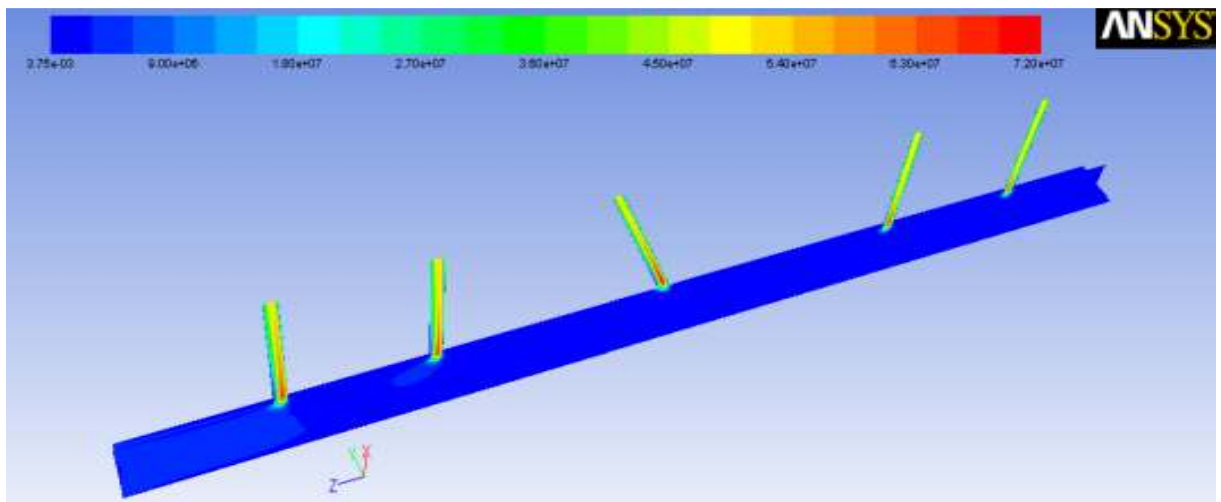
(b) Temperature of 300 K



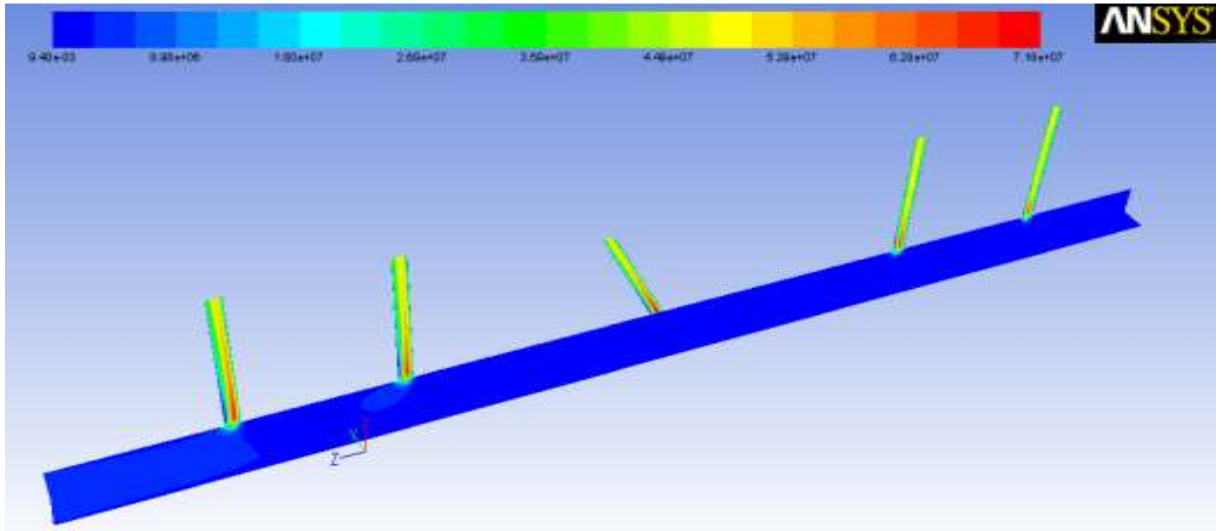
(c) Temperature of 310 K



(d) Temperature of 320 K

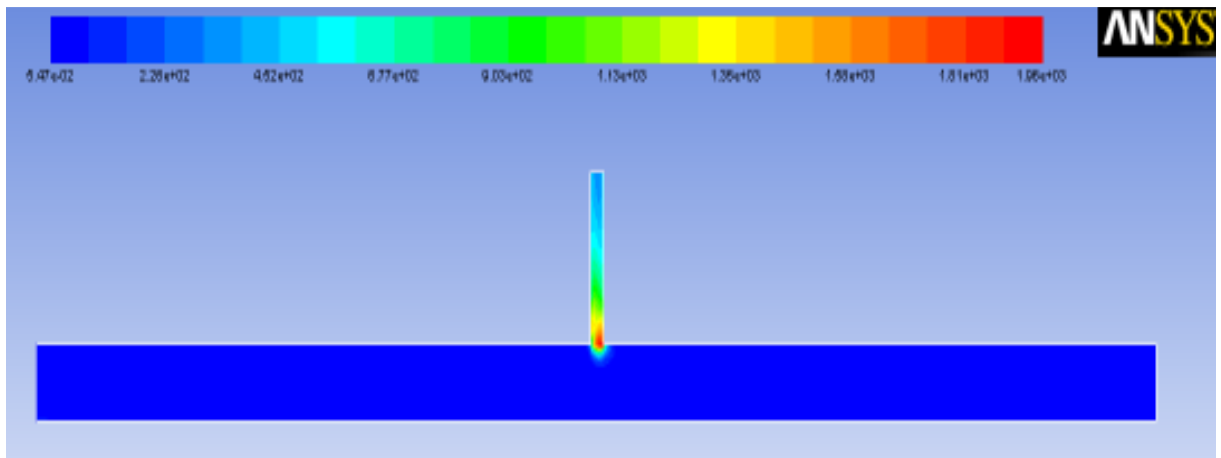


(e) Temperature of 330 K

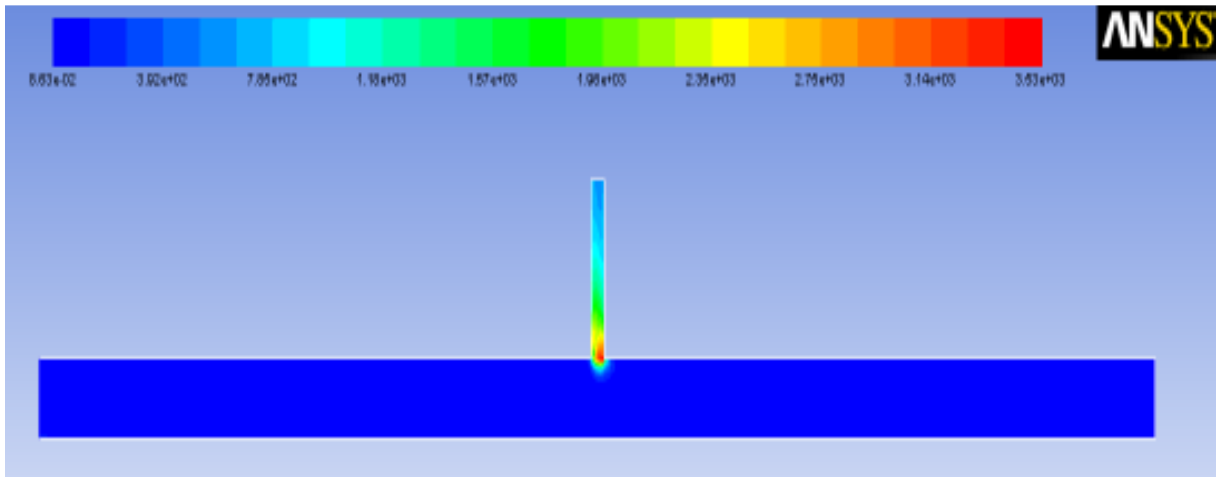


(f) Temperature of 340 K

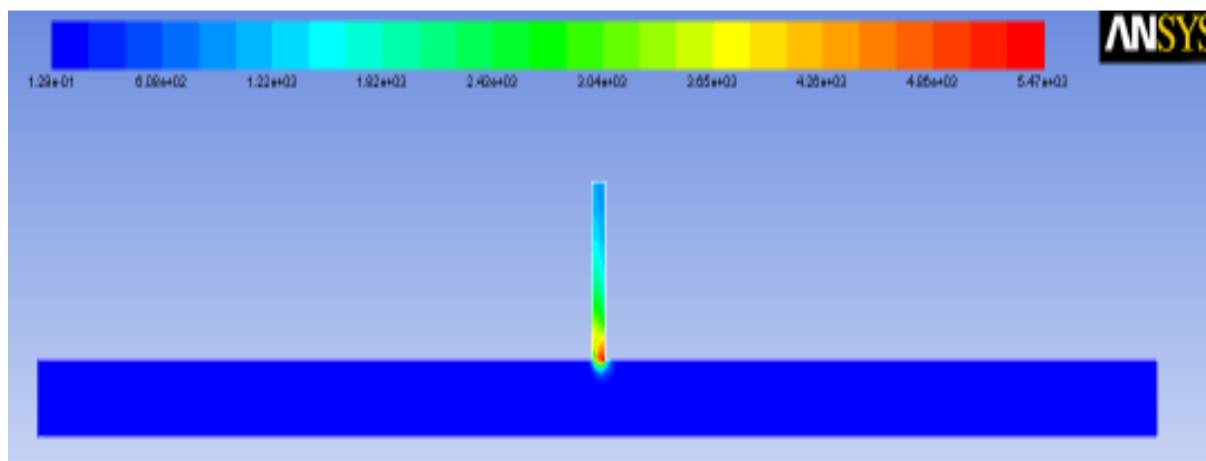
Fig. 5: Distributed cloud maps of dynamic pressure when five branches were processed synchronously at different temperatures



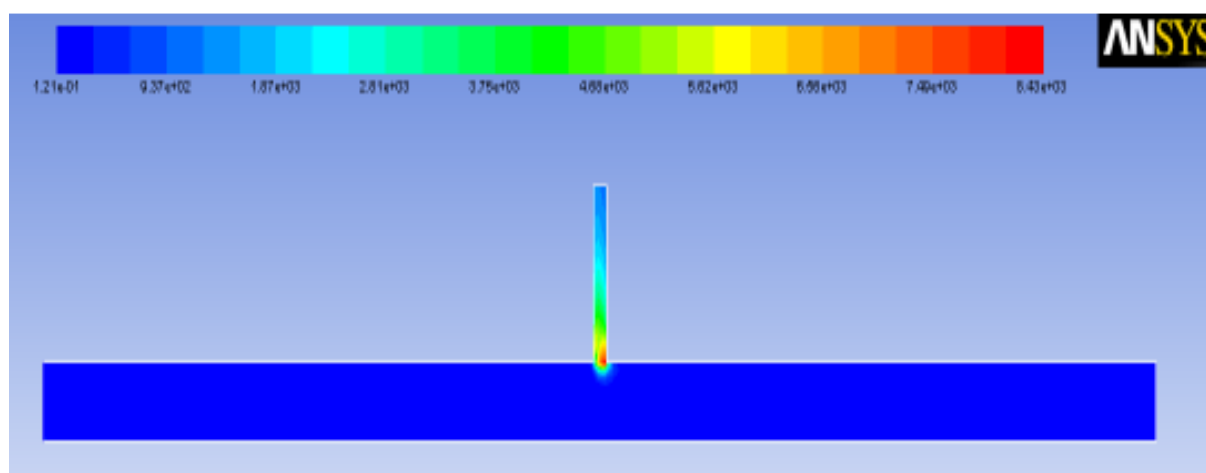
(a) Velocity of 30 m/s



(b) Velocity of 40 m/s



(c) Velocity of 50 m/s



(d) Velocity of 60 m/s

Fig. 6: Cloud maps of turbulence kinetic energy when only one branch was processed at different velocities

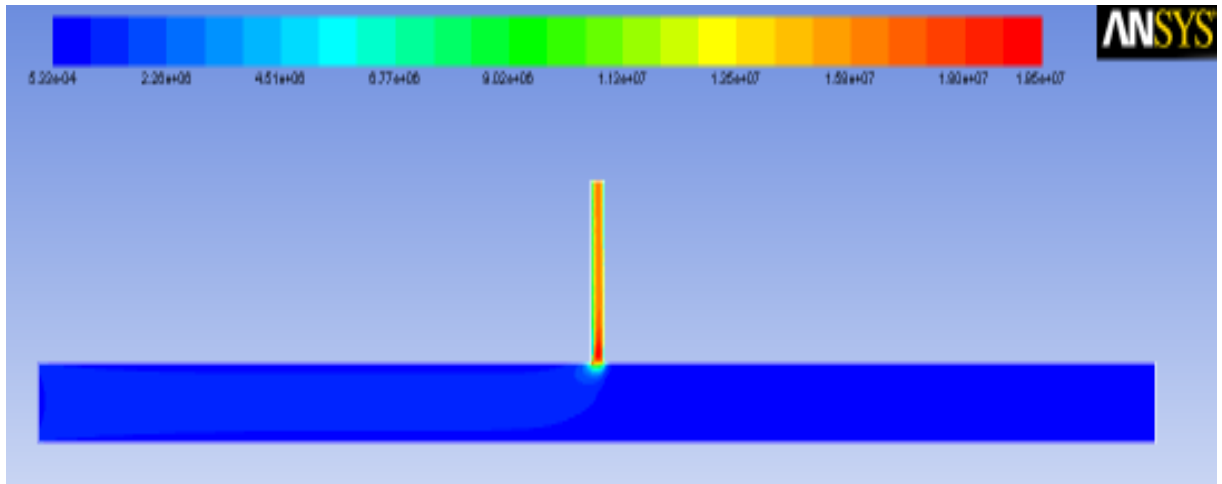
Table 1: Distribution of turbulence kinetic energy and dynamic pressure at regions close to the wall of common-rail branches when the velocity was 50 m/s

Temperature (K)	Turbulent kinetic energy (m <sup>2</sup> /s <sup>2</sup> )				Dynamic pressure (Mpa)			
	Section 1	Section 2	Section 3	Section 4	Section 1	Section 2	Section 3	Section 4
290	4 250	2 400	1 700	1 200	51	48	48	47
300	4 100	2 300	1 600	1 100	51	49	48	47
310	3 980	2 180	1 500	1 020	51	49	48	47
320	3 900	2 100	1 420	940	51	49	49	47
330	3 810	2 020	1 350	890	51.5	50	49	48
340	3 730	1 950	1 300	850	51	50	50	49

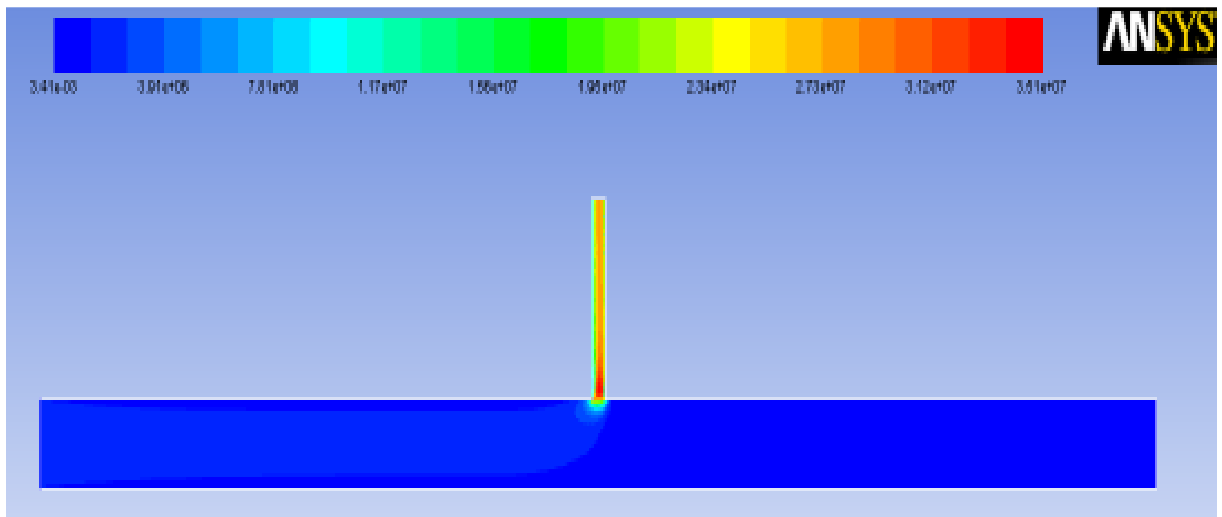
dynamic pressure at the regions close to the wall of common-rail branches is shown in Table 1.

Table 1 shows that the turbulence kinetic energy at regions close to the wall of common-rail branches declined as the working temperature increased. This was because the rise in temperature could result in a decline in the viscosity of abrasive flow of food molding, which could then reduce the resistance and velocity gradient of the abrasive flow of food molding. As a result, the turbulence pulse velocity generated there decreased and the turbulence kinetic energy at the

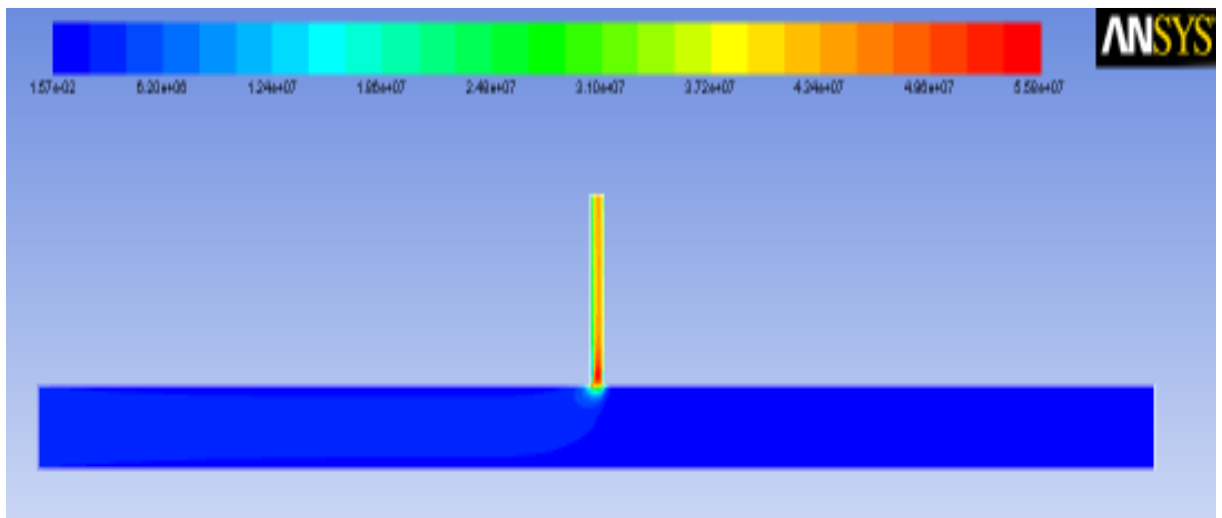
regions close to the wall of common-rail branches declined. Table 1 also shows that the turbulence kinetic energy gap between zone 1, 2, 3 and 4 was getting smaller and the turbulence kinetic energy at regions close to the wall of common-rail branches was not distributed evenly at any temperature. The change of temperature had an insignificant effect on the dynamic pressure at regions close to the wall of common-rail branches and the dynamic pressure at the outlet of branches was attenuated.



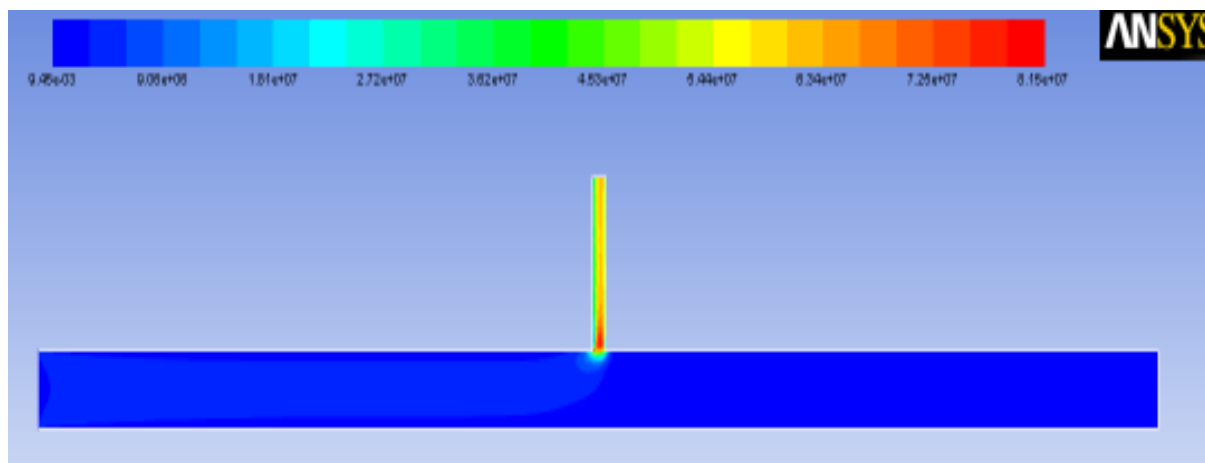
(a) Velocity of 30 m/s



(b) Velocity of 40 m/s



(c) Velocity of 50 m/s



(d) Velocity of 60 m/s

Fig. 7: Cloud maps of dynamic pressure when only one branch was processed at different velocities

Table 2: Distribution of the turbulence kinetic energy and dynamic pressure of common-rail branches when the temperature was 300 K

Velocity (m/s)	Turbulent kinetic energy (m <sup>2</sup> /s <sup>2</sup> )				Dynamic pressure (Mpa)			
	Section1	Section 2	Section 3	Section 4	Section 1	Section 2	Section 3	Section 4
30	3 487	1 697	1 007	509	49	47	45	44
40	3 790	1 990	1 290	788	50	48	47	46
50	4 100	2 300	1 600	1 100	51	50	49.5	49
60	4 405	2 600	1 880	1 350	51.5	50	49.5	49

In order to facilitate the comparative analyses, the process procedures in which only one branch was processed at different velocities were selected for study and only results on surface YOZ were displayed. When the initial temperature was 300 K, the simulation results of the turbulence kinetic energy and dynamic pressure at the main channel of common rail and the regions close to the wall of branches were analyzed.

Figure 6 shows that the turbulence kinetic energy of the micro holes in branches was much greater than that of the main channel and that it grew to a maximum at the cross hole. As the velocity of abrasive flow of food molding increased, the turbulence kinetic energy of regions close to the wall of branches also increased. This is caused by the sudden decrease in the cross section of branches and the sudden change of direction of abrasive flow of food molding. Both the increasing velocity of the flow in branches and the more intense random motion of the abrasive particles contributed to the increase in turbulence kinetic energy. It indicates that the turbulence kinetic energy distribution can be divided into 4 zones from the channel cross hole to the outlet, which are zone 1, 2, 3 and 4 from the bottom to the top.

Figure 7 shows the dynamic pressure distribution as follows: the dynamic pressure of the regions from the inlet to the cross hole at the channel center was greater than that of the regions close to the wall and it was higher at the center in the entire channel of branches and the maximum of the dynamic pressure also appeared at the cross hole; meanwhile, the

branches in the dynamic pressure maps were divided into 4 zones (zone 1, 2, 3 and 4) from the bottom to the top; according to the in-depth comparison of the turbulence kinetic energy and dynamic pressure of the regions close to the wall of common-rail branches, the distribution of the turbulence kinetic energy and dynamic pressure at the regions close to the wall of common-rail branches were obtained as shown in Table 2.

According to the analysis of the numerical results in Table 2, the turbulence kinetic energy increased as the velocity increased. When the inlet velocity was 50 m/s, it grew to a maximum. The turbulence kinetic energy in zone 1, 2, 3 and 4 did not change much compared with the case when the velocity was 40 m/s; after the inlet velocity reached 50 m/s, the velocities of 52, 55, 58 and 60 m/s, respectively were selected for the analysis of the abrasive flow of food molding machining values and the results show that the increment of turbulent kinetic energy declined again and the turbulence kinetic energy difference between zone 1, 2, 3 and 4 was getting larger. Therefore, when the inlet velocity was 50 m/s, the turbulence kinetic energy at the regions close to the wall of branches was well-distributed. By comparing the dynamic pressure values in Fig. 8, we can find that the dynamic pressure at the regions close to the wall of branches increased gradually along with the rise in inlet velocity and that the dynamic pressure difference between zone 1, 2, 3 and 4 was getting smaller, that is, the dynamic pressure was getting even in branches as the velocity increased. The comparative analysis shows that, when the inlet

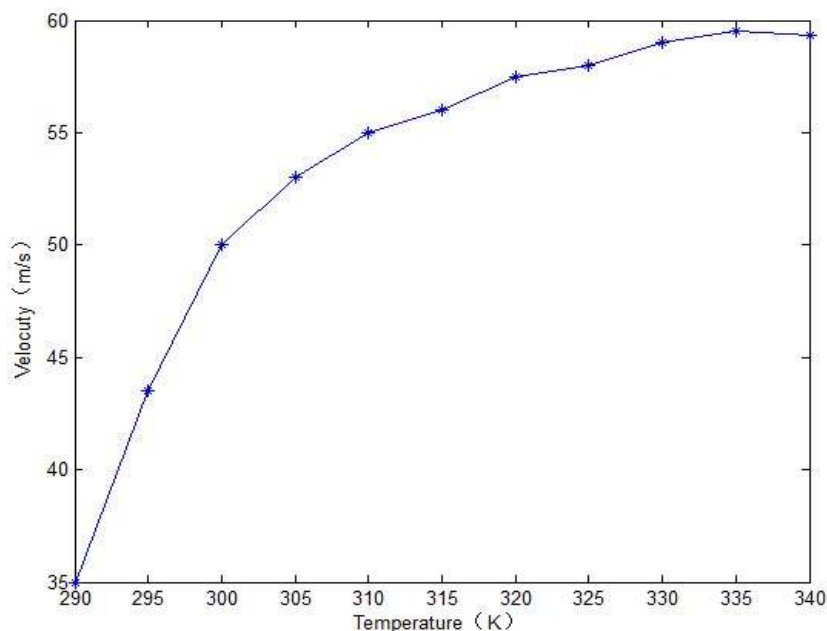


Fig. 8: Temperature-velocity graph of common-rail channel

velocity was 50 m/s, the dynamic pressure of branches was distributed evenly.

Based on the above analysis, we can conclude that the optimal machining velocity is 50 m/s when the temperature is 300 K, i.e., the optimal distribution of the dynamic pressure and turbulence kinetic energy at the regions close to the wall of common-rail branches will be achieved under such an initial condition. We can also work out the optimal initial velocities at temperatures of 290, 295, 305, 310, 315, 320, 325, 330, 335 and 340 K, respectively and draw the graphs of optimal velocity at different temperatures as shown in Fig. 8. Figure 8 shows that the optimal velocity increased by a large margin at the beginning as the temperature increased and then the velocity increment decreased gradually. This is because the increase of temperature can result in decline in the viscosity of abrasive flow of food molding and at that time, the influence of the velocity increase on the machining of abrasive flow of food molding in common-rail channel gets smaller.

### CONCLUSION

In accordance with the machining characteristics of abrasive flow of food molding and the parts structure of common-rail channel, the 3D simulation model was built. The numerical simulation of abrasive flow of food molding machining was performed with the application of the Fluent software and the pressure distribution and velocity distribution maps were obtained. The cases of the abrasive flow of food molding machining of different techniques were compared. The simulation results show that the practice of machining one branch separately with abrasive flow

of food molding facilitates the consistency in machining.

There is an optimal relation between velocity and temperature in abrasive flow of food molding machining. Under the simulation conditions in this study, a better machining quality was obtained when the optimal machining velocity was 50 m/s and the temperature was 300 K.

The cloud maps of static temperature, turbulence kinetic energy and dynamic pressure distribution in the flow field based on the numerical simulation can offer a theoretical basis to the quality control of abrasive flow of food molding machining.

### ACKNOWLEDGMENT

The authors would like to thank the national natural science foundation of china no. NSFC 51206011, Jilin province science and technology development program of Jilin province No. 20130522186JH and Doctoral Fund of Ministry of Education of China No. 20122216130001 for financially supporting this research under Contract.

### REFERENCES

- Jain, R.K. and V.K. Jain, 2000. Optimum selection of machining conditions in abrasive flow machining using neural network. *J. Mater. Process. Tech.*, 108: 62-67.
- Jain, R.K. and V.K. Jain, 2001. Specific energy and temperature determination in abrasive flow machining process. *Int. J. Mach. Tool. Manu.*, 41: 1689-1704.

- Jain, R.K. and V.K. Jain, 2004. Stochastic simulation of active grain density in abrasive flow machining. *J. Mater. Process. Tech.*, 152: 17-22.
- Li, J.Y., L.F. Yang, W.N. Li *et al.*, 2014. Research on nonlinear tube abrasive flow of food molding machining experiments. *China Mech. Eng.*, 25(13): 1729-1734.
- Liu, W., J.Y. Li, L.F. Yang, B. Liu, L. Zhao and B. Yu, 2012. Design analysis and experimental study of common rail abrasive flow machining equipment. *Adv. Sci. Lett.*, 5(2): 576-580.
- Sankar, M.R., V.K. Jain and J. Ramkumar, 2010. Rotational abrasive flow finishing (R-AFF) process and its effects on finished surface topography. *Int. J. Mach. Tool. Manu.*, 50: 637-650.
- Sankar, M.R., V.K. Jain and J. Ramkumar, 2011. Rheological characterization of styrene-butadiene based medium and its finishing performance using rotational abrasive flow finishing process. *Int. J. Mach. Tool. Manu.*, 51: 947-957.
- Walia, R.S., H.S. Shan and P. Kumar, 2008. Determining dynamically active abrasive particles in the media used in centrifugal force assisted abrasive flow machining process. *Int. J. Adv. Manuf. Technol.*, 38: 1157-1164.
- Zheng, W.J., J.Y. Li and G. Hao, 2012. Three-dimensional computer numerical simulation for micro-hole abrasive flow machining feature. *Int. Rev. Comput. Softw.*, 7(3): 1283-1287.